Electronic Supplementary Material (ESI) for Materials Chemistry Frontiers.

Electronic Supplementary Information

Superhydrophilic self-supported nickel/terbium oxide electrode for alkaline hydrogen evolution at high current density

Zining Qiu,[a] Xiaodan Yang,[a] Bowen Ni,[a] Jiarui Liu,[a] Hongming Sun,*[a] Jing Chen,[a] Cheng-Peng Li,[a] Miao Du*[b]

[a] Tianjin Key Laboratory of Structure and Performance for Functional Molecules, College of Chemistry, Tianjin Normal University, Tianjin 300387, China

E-mail: hxxyshm@tjnu.edu.cn

[b] College of Material and Chemical Engineering, Institute of New Energy Science and Technology, School of Future Hydrogen Energy Technology, Zhengzhou University of Light Industry, Zhengzhou 450001, China

E-mail: dumiao@zzuli.edu.cn

Experimental section

Chemicals

Ethanol (AR, CAS no. 64-17-5) and nickel nitrate (98%, CAS no. 13478-00-7) were purchased from Tianjin Damao Chemical Trading Co., Ltd. Potassium hydroxide (95%, CAS no. 1310-58-3), terbium nitrate (99.99%, CAS no. 57584-27-7), Pt/C (20%,CAS no. 7440-06-4) were purchased from Meryer (Shanghai) Chemical Technology Co., Ltd. Hydrochloric acid (36-38%, CAS no. 7647-01-0) and Nafion (D-521 dispersion 5% w/w in water & 1-propanol, CAS no. 31175-20-9) were purchased from Alfa Aesar. H_2 gas (99.99%) and Ar gas (99.999%) were purchased from Huanyu Co., Ltd. All chemicals were used as received without further purification.

Sample preparation

For preparation of Ni/Tb_2O_3 electrode, a graphite plate (1 × 2 cm^2) was cleaned in ethanol, dilute HCl and ultrapure water, respectively, which then was dried at room temperature. The precursor electrode was prepared by an electrodeposition method in an electrolytic cell with graphite plate as the working electrode. The deposited electrolyte was a water solution of 0.09 M $Ni(NO_3)_2$ and 0.01 M $Tb(NO_3)_3$. During the electrodeposition process of $Ni(OH)_2$/$Tb(OH)_3$, the GP was treated at 40 mA cm^{-2} for 600 s and then −40 mA cm^{-2} for 600 s. Subsequently, the deposited $Ni(OH)_2$/$Tb(OH)_3$ was converted to Ni/Tb_2O_3 in a tube furnace at 500 °C under 10% H_2/Ar mixture for 2 h with a heating rate of 5 °C min^{-1}. For comparison, Ni/Tb_2O_3 with different Ni:Tb molar ratios (i.e. 99:1, 97:3, 95:5, 90:10, 80:20 and 70: 30) were synthesized by adjusting the amount of $Ni(NO_3)_2$ and $Tb(NO_3)_3$. In addition, the Ni and Tb_2O_3 electrodes were prepared similarly. The catalyst loading is ca. 3.5 mg cm^{-2} for each electrode.

In the electrodeposition process, the nitrate anion in electrolyte was firstly inserted into the interlayers of graphitic substrate. Then, the nitrate anion was reduced to yield OH^-, increasing the local pH value near the electrode and thus leading to the formation of $Ni(OH)^2$ and $Tb(OH)^3$.With the NO_3^- intercalation process, the deposited $Ni(OH)_2$ and $Tb(OH)_3$ could form firm deposit–substrate interaction with the graphite substrate, which could lower interface resistance and improve the stability of the loaded catalysts. The reactions involved are as follows:

$NO_3^- + H_2O + 2e^- = NO_2^- + 2OH^-$ (E^θ = 0.838 V)

$Ni^{2+} + 2OH^- = Ni(OH)_2 \downarrow$

$Tb^{3+} + 3OH^- = Tb(OH)_3 \downarrow$

Characterizations

Powder XRD patterns were taken on a Rigaku model Ultima IV diffractometer with Cu-Kα X-ray source. SEM images were performed on a FEI Nova Nano 230 scanning electron microscope. TEM equipped with EDS and SAED was conducted on a Tecnai G2 F20 electron microscope. XPS was taken by a Kratos Axis Ultra DLD spectrometer.

Inductively coupled plasma atomic emission spectrometer (ICP-AES) was performed on PerkinElmer Optima 83000.

Electrochemical measurements

Electrochemical measurements were taken in a three-electrode cell with a volume of 150 mL by using the Bipotentiostat workstation (Pine Research Instrumentation, Basic Wave Driver 20 Bundle, USA) and Solartron ModuLab XM. The as-prepared self-supported electrode was used as the working electrode. The area of as-prepared electrode is 2.0 cm^2, of which the part loading catalyst immersed into the electrolyte is 1.0 cm^2 (Fig. S1, ESI). The Pt/C(20%)@GP electrode was prepared by drop casting Pt/C(20%) catalyst ink onto GP (3.5 mg cm^{-2}). The ink was achieved by ultrasonically dispersing 5 mg Pt/ C(20%) in a mixed solution containing 450 µL ethanol and 50 µL Nafion solution. 1.0 M KOH was used as the electrolyte. The LSV plots were recorded at a rate of 10 mV s^{-1}. EIS measurements were taken in the frequency region from 100 kHz to 0.01 Hz. The amounts of produced H_2 were collected using the drainage route. The Faradic efficiency was defined as the ratio of experimental H_2 production amount to theoretical H_2 production amount. All potentials were reported relative to the RHE scale unless noted. All polarization curves were iR-corrected with $E_{iR} = E_{tested} – i \times 0.6R_s$ (R_s is resistance of system).

Turnover frequency (TOF) calculation

The per-site TOF values can be calculated based on the following equation.

$$TOF = \frac{\#\ total\ hydrogen\ turnover/cm^2\ geometric\ area}{\#\ active\ sites/cm^2\ geometric\ area}$$

The number of total hydrogen turnovers is calculated from the current density:

$$\#\ H_2 = (j\frac{mA}{cm^2})(\frac{1C/s}{1000\ mA})(\frac{1mol\ e^{-1}}{96485.3\ C})(\frac{1mol\ H_2}{2mol\ e^{-1}})(\frac{6.02 \times 10^{23}\ molecules\ H_2}{1mol\ H_2}) = 3.12 \times 10^{15}\frac{H_2/s}{cm^2}\ per\ \frac{mA}{cm^2}$$

Given the great difficulty of determining the exact quantity of active sites on catalyst surface, especially for such hybrid catalysts with interface in this work, we assume the total number of surface Ni sites as the number of active sites, which are estimated by the reported method. Molar mass of Ni: 58.69 g mol^{-1}; Density of Ni: 8.90 g cm^{-3}; Molar volume of Ni: 6.60 cm^3 mol^{-1}. Average surface atoms per 1 square centimeter:

$$\#\ suface\ sites = (j\frac{3.12 \times 10^{15}\frac{H_2/s}{cm^2}}{1\ mol} \times \frac{1\ mol}{6.60\ cm^2})^{\frac{2}{3}} = 2.03 \times 10^{15}\frac{atoms}{cm^2}$$

Then, the current density from the LSV polarization curves can be converted into TOF values according to:

$$TOF = \frac{(3.12 \times 10^{15}\frac{H_2/s}{cm^2}\ per\ \frac{mA}{cm^2}) \times |j|}{(\#\ ac\#\ suface\ sites) \times A_{ECSA}}$$

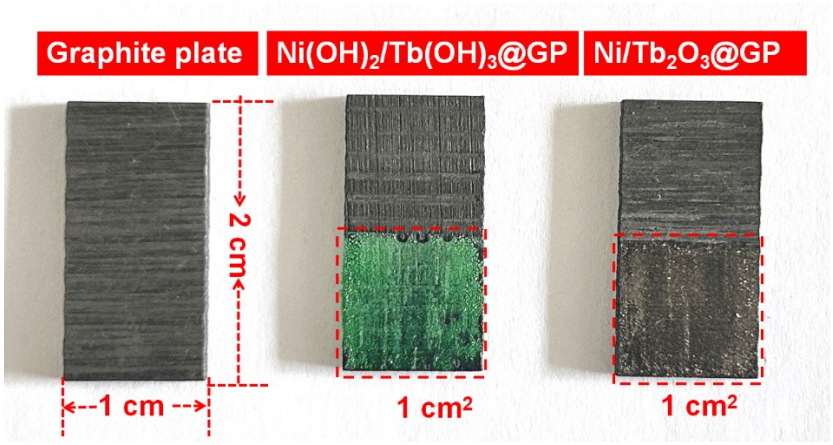

Fig. S1 Optical images of electrodes. (Left) graphite plate (GP), (middle) $Ni(OH)_2/Tb(OH)_3$@GP and (right) Ni/Tb_2O_3@GP electrodes.

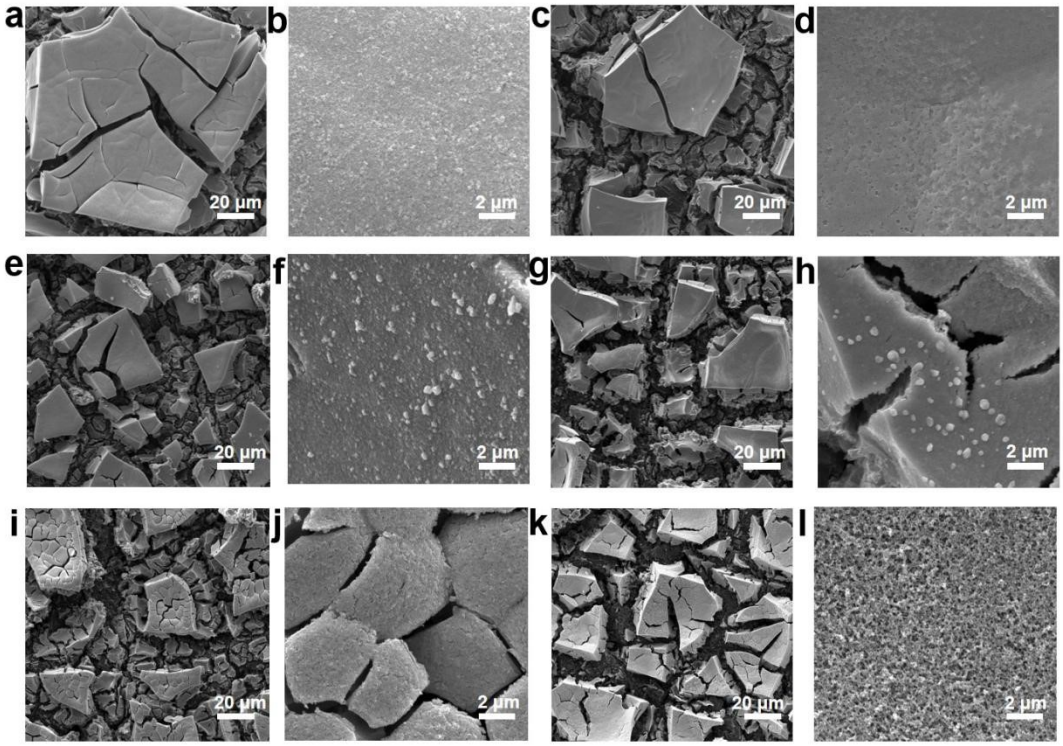

Fig. S2 SEM images of at low and high magnifications, respectively. **a**, **b** Ni/Tb_2O_3@GP-70:30. **c**, **d** Ni/Tb_2O_3@GP-80:20. **e**, **f** Ni/Tb_2O_3@GP-90:10. **g**, **h** Ni/Tb_2O_3@GP-95:5. **i, j** Ni/Tb_2O_3@GP-97:3. **k, l** Ni/Tb_2O_3@GP-99:1.

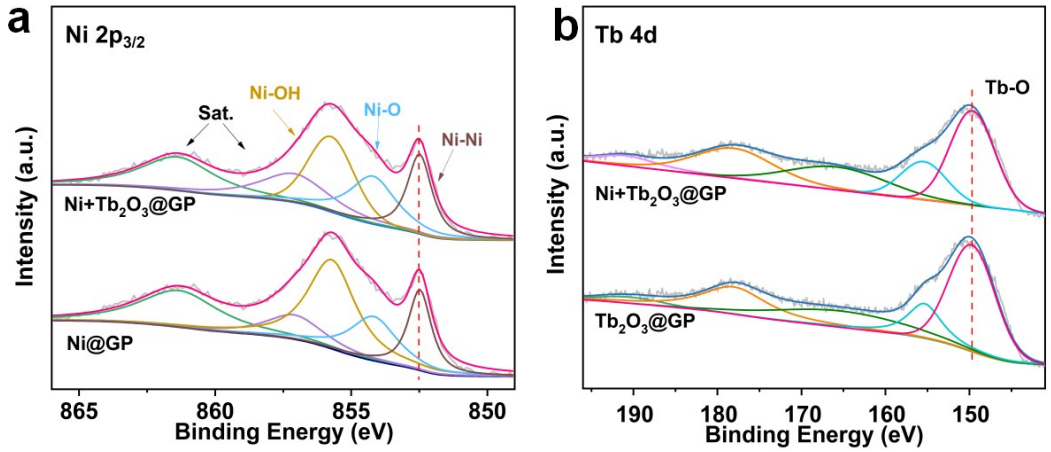

Fig. S3 XPS spectra of Ni+Tb_2O_3@GP. **a** Ni 2p XPS spectrum. **b** Tb 4d XPS spectrum.

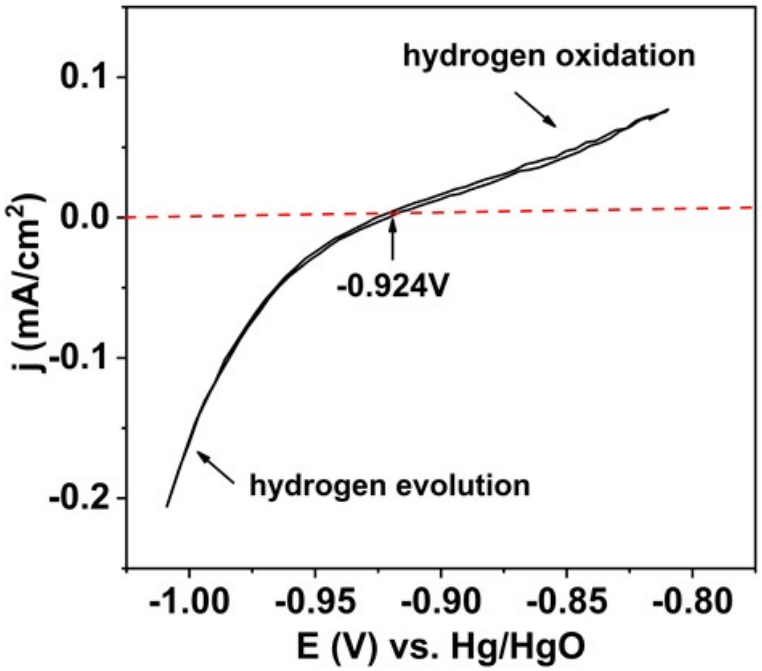

Fig. S4 Potential calibration of reference electrode in H_2-saturated 1.0 M KOH solution. CV curves of platinum plate electrode recorded at a scan rate 5 mV s^{-1}. The CV result of RHE calibration: E(RHE) = E(SCE) + 0.924 V.

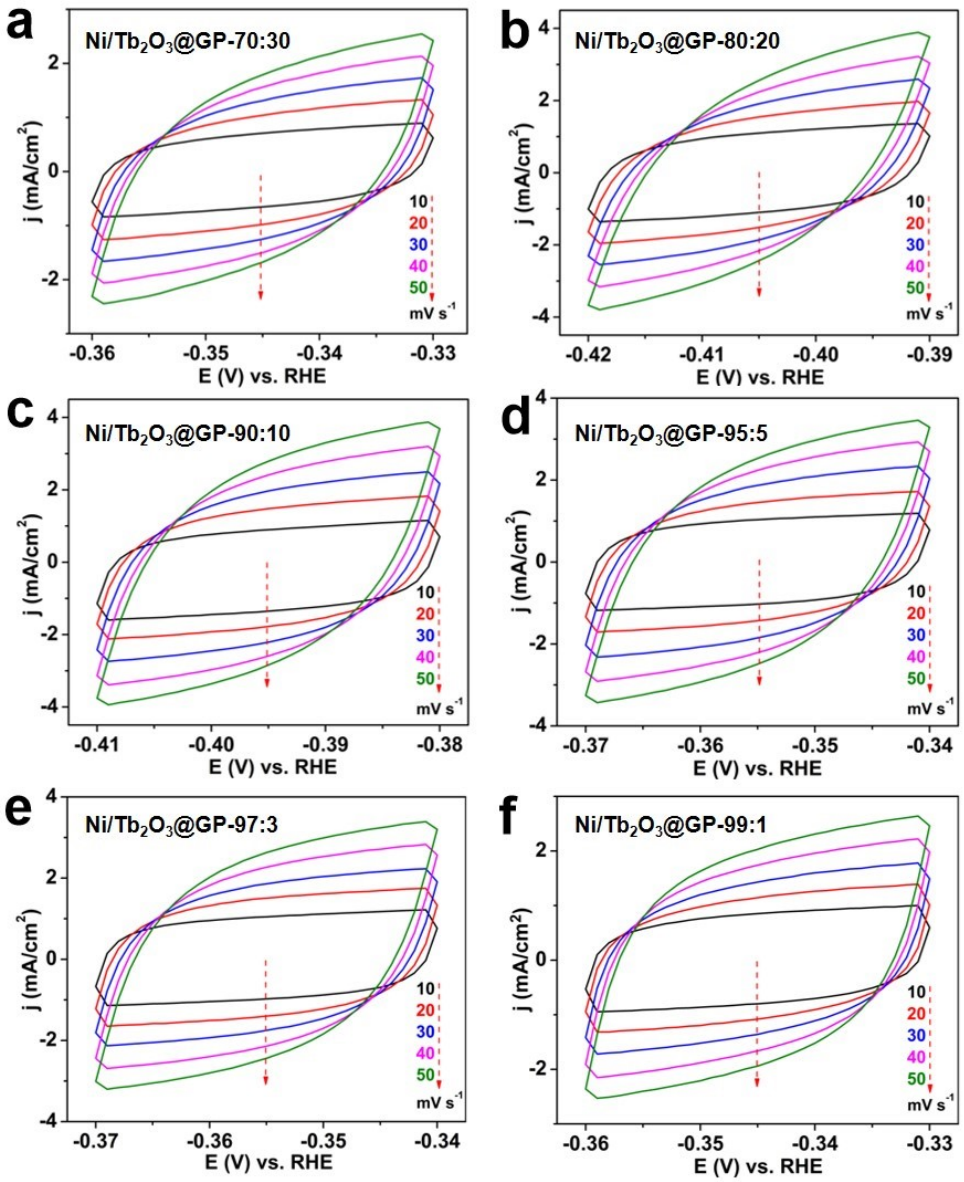

Fig. S5 Double-layer capacitance (C_{dl}) measurements in 1 M KOH. CV curves at different scan rates within the non-Faradaic potential range for **a** Ni/Tb_2O_3@GP-70:30, **b** Ni/Tb_2O_3@GP-80:20, **c** Ni/Tb_2O_3@GP-90:10, **d** Ni/Tb_2O_3@GP-95:5, **e** Ni/Tb_2O_3@GP-97:3 and **f** Ni/Tb_2O_3@GP-99:1.

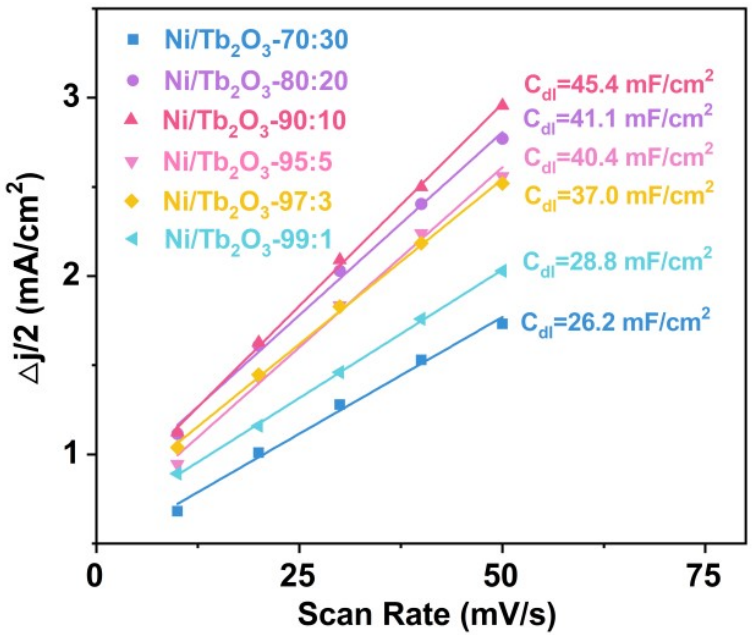

Fig. S6 Double-layer capacitance (C_{dl}). Capacitive currents on the basis of scan rate for Ni/Tb_2O_3@GP electrodes with different Ni:Tb molar ratios.

The ECSA was determined assuming a general specific C_{dl} capacitance of 40 mF cm^{-2} for all samples.

$$\#\ A_{ECSA}^{Sample} = \frac{Specific\ capacitance(\mu F\ cm^{-2}\ )}{40\ \mu F\ cm^{-2}\ per\ cm_{ECSA}^{2}}$$

$$A_{ECSA}^{Ni/Tb_2O_3@GP-70:30} = \frac{26.2mF\ cm^{-2}}{40\ \mu F\ cm^{-2}\ per\ cm_{ECSA}^{2}} = 655\ cm_{ECSA}^{2}$$

$$A_{ECSA}^{Ni/Tb_2O_3@GP-80:20} = \frac{41.1mF\ cm^{-2}}{40\ \mu F\ cm^{-2}\ per\ cm_{ECSA}^{2}} = 1027.5\ cm_{ECSA}^{2}$$

$$A_{ECSA}^{Ni/Tb_2O_3@GP-90:10} = \frac{45.4mF\ cm^{-2}}{40\ \mu F\ cm^{-2}\ per\ cm_{ECSA}^{2}} = 1135\ cm_{ECSA}^{2}$$

$$A_{ECSA}^{Ni/Tb_2O_3@GP-95:5} = \frac{40.4mF\ cm^{-2}}{40\ \mu F\ cm^{-2}\ per\ cm_{ECSA}^{2}} = 1010\ cm_{ECSA}^{2}$$

$$A_{ECSA}^{Ni/Tb_2O_3@GP-97:3} = \frac{37.0mF\ cm^{-2}}{40\ \mu F\ cm^{-2}\ per\ cm_{ECSA}^{2}} = 925\ cm_{ECSA}^{2}$$

$$A_{ECSA}^{Ni/Tb_2O_3@GP-99:1} = \frac{28.8mF\ cm^{-2}}{40\ \mu F\ cm^{-2}\ per\ cm_{ECSA}^{2}} = 720\ cm_{ECSA}^{2}$$

The A_{ECSA} of Ni/Tb_2O_3@GP-90:10 was calculated to be 1135 cm^2 $_{ECSA}$ and the TOF value of Ni/Tb_2O_3@GP-90:10 was calculated to be TOF (100 mV) = 0.691 s^{-1}.

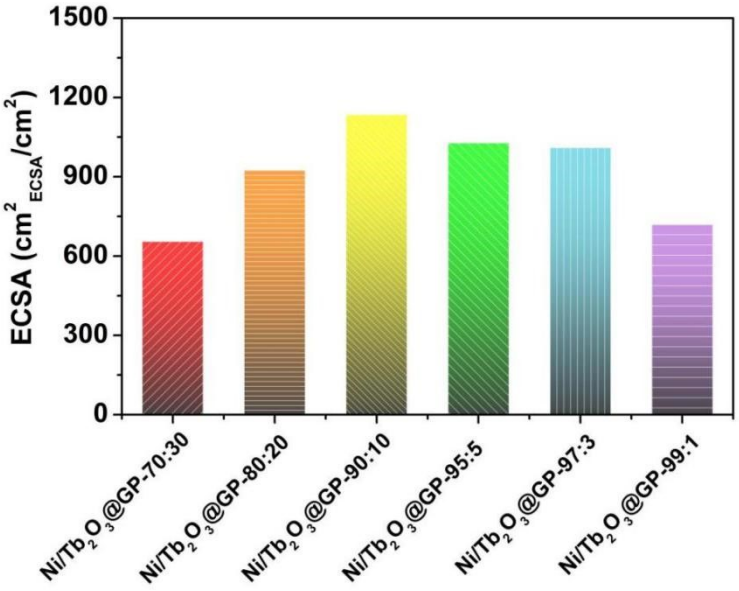

Fig. S7 Comparison of ECSAs for Ni/Tb_2O_3@GP electrodes with different Ni/Tb molar ratios.

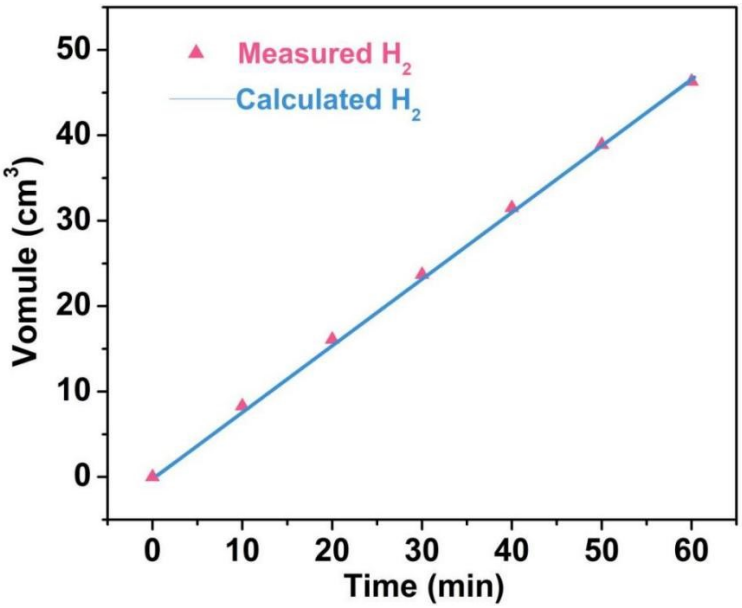

Fig. S8 Generated and theoretical volumes of H_2 gas over time at 100 mA cm^{-2} for Ni/Tb_2O_3@GP.

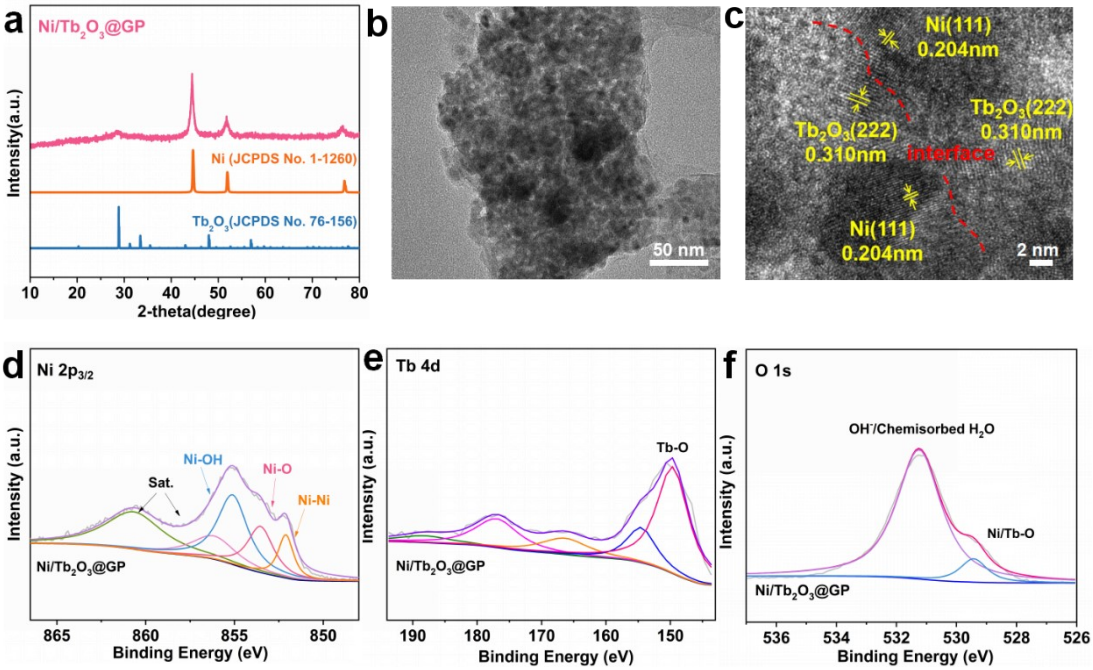

Fig. S9 Characterization of used Ni/Tb_2O_3@GP electrode after HER test. **a** XRD. **b** TEM image. **c** HRTEM image. **d** Ni 2p XPS spectrum. **e** Tb 4d XPS spectrum. **f** O 1s XPS spectrum.

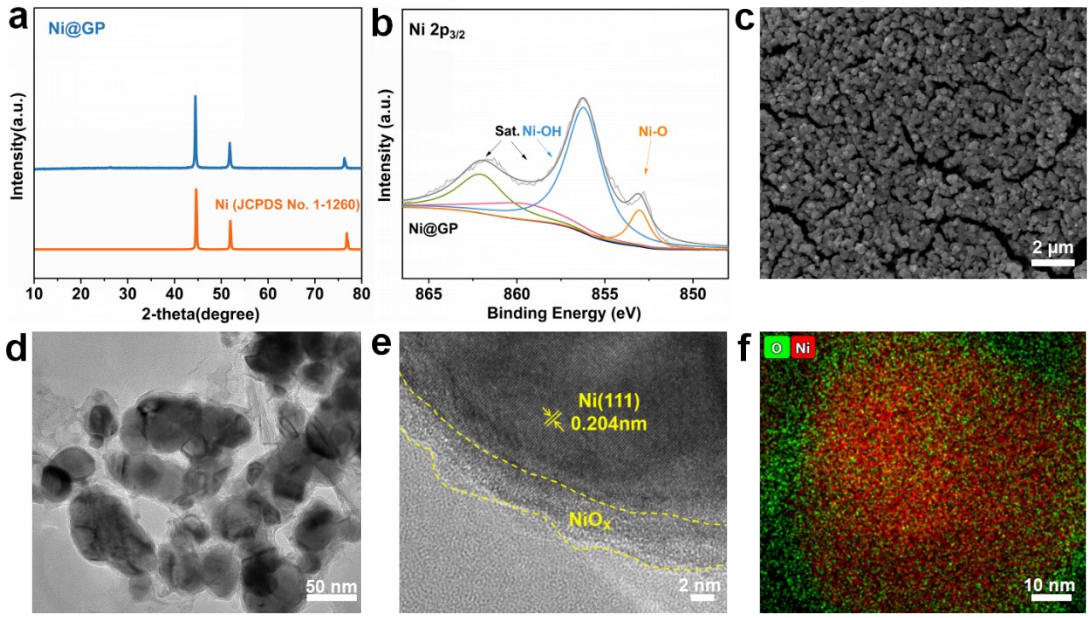

Fig. S10 Characterization of used Ni@GP electrode after HER test. **a** XRD. **b** Ni 2p XPS spectrum. **c** SEM image. **d** TEM image. **e** HRTEM image. **f** TEM-EDX elemental mapping.

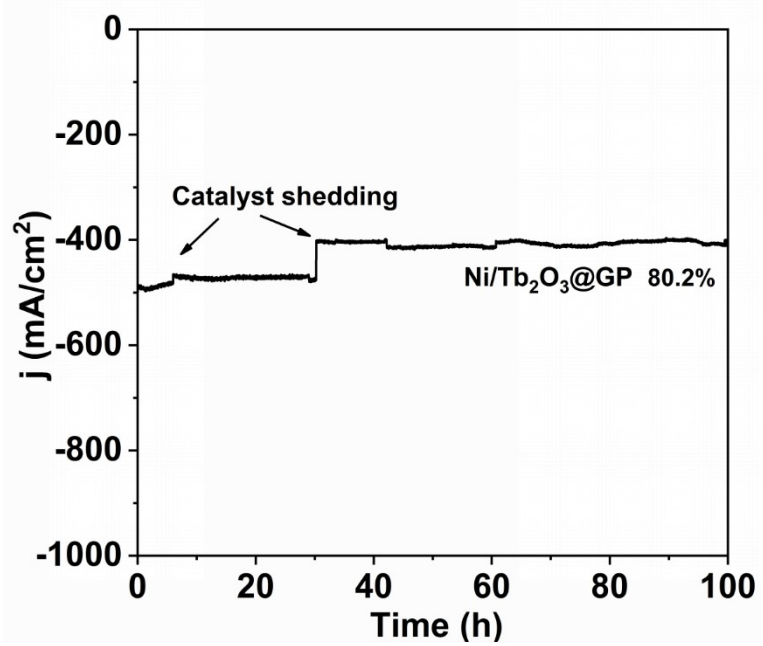

Fig. S11 Stability test of Ni/Tb_2O_3@GP-2 at the overpotential of 816 mV.

Table 1. Compositions of Ni/Tb_2O_3@GP electrodes with different Ni:Tb molar ratios determined by ICP-AES.

Sample	Ni (atom%)*	Tb (atom%)*
Ni/Tb_2O_3@GP-70:30	69.27 ± 1.94	30.73 ± 1.94
Ni/Tb_2O_3@GP-80:20	80.12 ± 0.94	19.88 ± 0.94
Ni/Tb_2O_3@GP-90:10	89.97 ± 1.56	20.03 ± 1.56
Ni/Tb_2O_3@GP-95:5	95.45 ± 2.04	4.55 ± 2.04
Ni/Tb_2O_3@GP-97:3	96.78 ± 1.25	3.22 ± 1.25
Ni/Tb_2O_3@GP-99:1	98.81± 2.72	1.29 ± 2.72

***** The error bars represent the standard derivation based on triplicate measurements.

Table 2. Comparison of the electrocatalytic HER activities for Ni/Tb_2O_3@GP and reported nonprecious catalysts in 1.0 M KOH electrolyte.

Catalyst	η_{-10}(mV)	Tafel slope (mV dec^{-1})	Substrate	Stability
This work	71.4	43.9	graphite plate	-500 mA cm^{-2}@360 h
Ni_3N nanosheets/Pt[1]	50	36.5	Carbon cloth	-10 mA cm^{-2}@20 h
Ni_5P_4 film/NF[2]	150	53	Ni foam	-10 mA cm^{-2}@20 h
$NiP_2/NiSe_2$[3]	89	65.7	Carbon fibers	-10 mA cm^{-2}@90 h
$NiSe_2$[4]	157	67	Carbon paper	-10 mA cm^{-2}@24 h
Ni-N_x/porous carbon[5]	147	114	-	-10 mA cm^{-2}@10 h
Cu nanodot decorated Ni_3S_2 nanotubes[6]	128	76.2	Carbon fibers	-10 mA cm^{-2}@20 h
Ni_3N_{1-x}/NF[7]	55	54	Ni foam	-50 mA cm^{-2}@50 h
$Co(OH)_2$-MoS_2[8]	89	53	Glassy carbon	-10 mA cm^{-2}@20 h
Ni-Ni_3C[9]	98	88.5	Carbon cloth	-35 mA cm^{-2}@35 h
1T–$MoS_2/M(OH)_2$[10]	57	30	Carbon fiber	-500 mA cm^{-2}@100 h
Ni-$Ni(OH)_2$[11]	72	43	Ni foam	-10 mA cm^{-2}@28 h
$MoS_2/CoNi_2S_4$[12]	78	67.4	Carbon fibers	-10 mA cm^{-2}@48 h
Co/Se-MoS_2-NF[13]	98	67	Ni Foam	-1000 mA cm^{-2}@360 h
$NiCu_x/Ni_3S_2$[14]	202	86	Ti mesh	-10 mA cm^{-2}@11 h
MoC-Mo_2C-790[15]	68	59	Mo tablet	-30 mA cm^{-2}@1000 h
F,P-Fe_3O_4/IF[16]	121	127.9	Iron mesh	-500 mA cm^{-2}@12 h
MoO_2-FeP[17]	103	48	FeOOH	-10 mA cm^{-2}@24 h
CoP/NiCoP[18]	133	88	Ti foil	-20 mA cm^{-2}@24 h

References

1. Y. Wang, L. Chen, X. Yu, Y. Wang and G. Zheng, Superb alkaline hydrogen evolution and simultaneous electricity generation by Pt-decorated Ni_3N nanosheets, *Adv. Energy Mater.*, 2017, **7**, 1601390.
2. M. Ledendecker, K. Calderón, S. Papp, C. Steinrück, H. P. Antonietti and M. Shalom, The synthesis of nanostructured Ni_5P_4 films and their use as a non-noble bifunctional electrocatalyst for full water splitting, *Angew. Chem., Int. Ed.,* 2015, **54**, 12361-12365.
3. L. Yang, L. Huang, Y. Yao and L. Jiao, In-situ construction of lattice-matching $NiP_2/NiSe_2$ heterointerfaces with electron redistribution for boosting overall water splitting, *Appl. Catal. B. Environ.,* 2020, **282**, 119584.
4. L. Zhai, T. W. B. Lo, Z.-L. Xu, J. Potter, J. Mo, X. Guo, C. C. Tang, S. C. E. Tsang and S. P. Lau, In situ phase transformation on nickel-based selenides for enhanced hydrogen evolution reaction in alkaline medium, *ACS Energy Lett.,* 2020, **5**, 2483-2491.
5. C. Lei, Y. Wang, Y. Hou, P. Liu, J. Yang, T. Zhang, X. Zhuang, M. Chen, B. Yang, L. Lei, C. Yuan, M. Qiu and X. Feng, Efficient alkaline hydrogen evolution on atomically dispersed $Ni\text{-}N_x$ species anchored porous carbon with embedded Ni nanoparticles by accelerating water dissociation kinetics, *Energy Environ. Sci.*, 2019, **12**, 149-156.
6. J. Feng, J. Wu, Y. Tong and G. Li, Efficient hydrogen evolution on Cu nanodots-decorated Ni_3S_2 nanotubes by optimizing atomic hydrogen adsorption and desorption, *J. Am. Chem. Soc.,* 2018, **140**, 610-617.
7. B. Liu, B. He, H. Peng, Y. Zhao and W. Zhang, Unconventional nickel nitride enriched with nitrogen vacancies as a high efficiency electrocatalyst for hydrogen evolution, *Adv. Sci.,* 2018, **5**, 1800406.
8. Y. Luo, X. Li, X. Cai, X. Zou, F. Kang, H.-M. Cheng and B. Liu, Two-dimensional MoS_2 confined $Co(OH)_2$ electrocatalysts for hydrogen evolution in alkaline electrolytes, *ACS Nano.*, 2018, **12**, 4565-4573.
9. P. Wang, R. Qin, P. Ji, Z. Pu and S. Mu, Synergistic coupling of Ni nanoparticles with Ni_3C nanosheets for highly efficient overall water splitting, *Small,* 2020, **16**, 2001642.
10. W. Chen, J. Gu, Y. Du, F. Song, F. Bu, J. Li, Y. Yuan, R. Luo, Q. Liu and D. Zhang, Achieving rich and active alkaline hydrogen evolution heterostructures via interface engineering on 2D 1T-MoS_2 quantum sheets, *Adv. Funct. Mater.,* 2020, **30**, 2000551.
11. W. Zhong, W. Li, C. Yang, J. Wu and R. Zhao, Interfacial electron rearrangement: Ni activated $Ni(OH)_2$ for efficient hydrogen evolution, *J. Energy Chem.,* 2021, **61**, 236-242.
12. J. Hu, C. Zhang, P. Yang, J. Xiao, T. Deng, Z. Liu, B. Huang, M. K. H. Leung and S. Yang, Kinetic-oriented construction of MoS synergistic interface to boost pH-universal hydrogen evolution, *Adv. Funct. Mater.*, 2020, **30**, 1908520.
13. Z. Zheng, L. Yu, M. Gao, X. Chen, W. Zhou, C. Ma, L. Wu, J. Zhu, X. Meng, J. Hu, Y. Tu, S. Wu, J. Mao, Z. Tian and D. Deng, Boosting hydrogen evolution on MoS_2 via co-confining selenium in surface and cobalt in inner layer, *Nat. Commun.,* 2020, **11**, 3315.
14. H. Du, R. Kong, F. Qu and L. Lu, Enhanced hydrogen evolution activity of Ni/Ni_3S_2 nanosheet grown on Ti mesh by Cu doped Ni, *J. Electrochem, Soc.,* 2019, **166**, 168-173.
15. W. Liu, X. Wang, F. Wang, K. Du, Z. Zhang, Y. Guo, H. Yin and D. Wang, A durable and pH-universal self-standing MoC–Mo_2C heterojunction electrode for efficient hydrogen evolution reaction, *Nat. Commun.,* 2019, **12**, 6776.

16. J. Zen, X. Shang, H. Ren, J. Hi, H. Fu, B. Dong, C. Liu and Y. Chai, Modulation of inverse spinel Fe_3O_4 by phosphorus doping as an industrially promising electrocatalyst for hydrogen evolution, *Adv. Mater.,* 2019, **19**, 05107.
17. G. Yang, Y. Jiao, H. Yan, Y. Xie, A. Wu, X. Dong, D. Guo, C. Tian and H. Fu, Interfacial engineering of MoO_2-FeP heterojunction for highly efficient hydrogen evolution coupled with biomass electrooxidation, *Adv. Mater.,* 2020*,* **32**, 2000455.
18. Y. Lin, K. Sun, S. Liu, X. Chen, Y. Cheng, W. Cheong, Z. Chen, L. Zheng, J. Zhang, X. Li, Y. Pan and C. Chen, Construction of CoP/NiCoP nanotadpoles heterojunction interface for wide pH hydrogen evolution electrocatalysis and supercapacitor, *Adv. Energy Mater.,* 2019, **9**, 1901213.